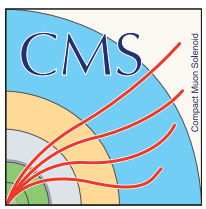
Entanglement measurements at CMS and ATLAS

Leyun Gao (on behalf of the CMS and ATLAS Collaborations)

Peking University

DISCRETE 2026







A brief history of entanglement and Bell tests

- Entanglement $\rightarrow$ a joint state that cannot be written as a mixture of product states.
- EPR questioned the completeness of quantum mechanics under locality; Bell derived inequalities for local hidden-variable theories (LHVTs).
- Quantum mechanics predicts, and photon experiments have observed, violations of these inequalities.
- Collider measurements probe entanglement under model-dependent assumptions, but can not constitute rigorous Bell tests (JHEP 08 (2026) 067).

1935
EPR: completeness and locality

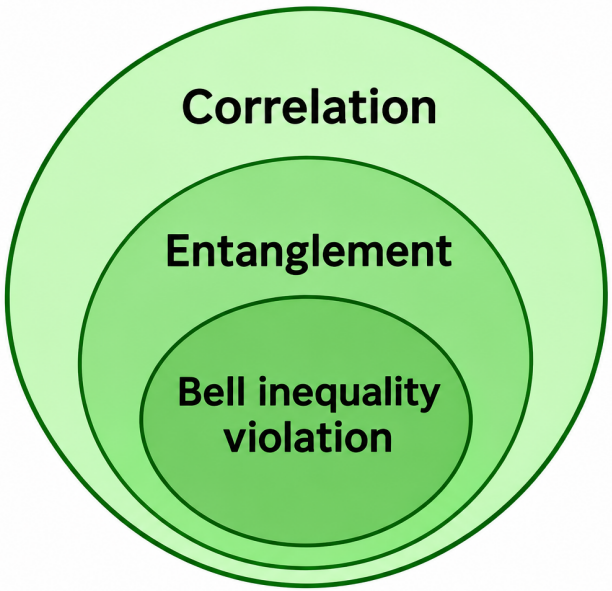
1964
Bell inequalities for local theories

1972
Freedman–Clauser: first photon Bell test

2022
Nobel Prize for Bell tests

2024 onward
LHC: entanglement in top and Higgs events

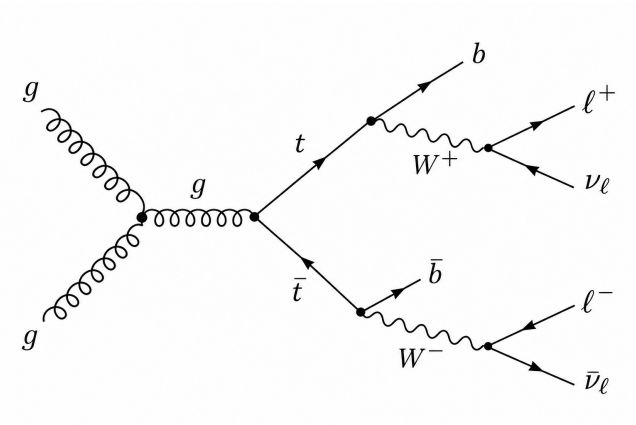
Correlation, entanglement, and Bell inequality violation



- Correlation: Statistical dependence between measurement outcomes.
- Entanglement: Quantum correlations due to nonseparability of a joint state.
- Bell inequality violation: Correlations incompatible with any LHVT.

$t\bar{t}$: a powerful probe of quantum entanglement at the energy frontier

Nature 633 (2024) 542–547



- A $t\bar{t}$ pair forms a two-qubit system. Near the production threshold, $\sim 80\%$ are in a spin-singlet state, with entanglement preserved after averaging over production directions.
- The top quark decays before hadronization and spin decorrelation, transferring its spin information to its decay products ($|\kappa_\ell| \sim 1$).

- The large number of $t\bar{t}$ events at the LHC enables detailed studies of quantum correlations.
- The spin-correlation matrix $\mathbf{C}$ provides an entanglement witness:

$$D = \frac{\mathrm{tr}[\mathbf{C}]}{3} = -3\langle \cos\varphi \rangle,$$

where φ is the angle between the charged leptons in their parent top-quark rest frames.

- $D < -1/3$ signals entanglement. An inclusive measurement can dilute this signal, motivating a dedicated near-threshold analysis.

Outline

- ATLAS, Nature 633, 542–547 (2024): first observation of $t\bar{t}$ entanglement near threshold.
- CMS, Rep. Prog. Phys. 87, 117801 (2024): independent threshold observation, including a study of toponium-like effects.
- CMS, Phys. Rev. D 110, 112016 (2024): differential spin correlations, high-mass entanglement, and a critical-entanglement test.
- CMS, Phys. Rev. D 113, L051101 (2026): beam-basis measurements and broader top-pair state characterization.
- CMS-PAS-TOP-23-006 (2026): 38 angular observables measuring the dilepton spin-density structure differentially.
- CMS-PAS-HIG-25-011 (2025); Phys. Rev. Lett. 137, 111804 (2026): entanglement established in $H \to ZZ^* \to 4\ell$.

ATLAS $t\bar{t}$ entanglement observation: detector-level results

Nature 633 (2024) 542–547, 140 fb^{-1} at $\sqrt{s} = 13$ TeV

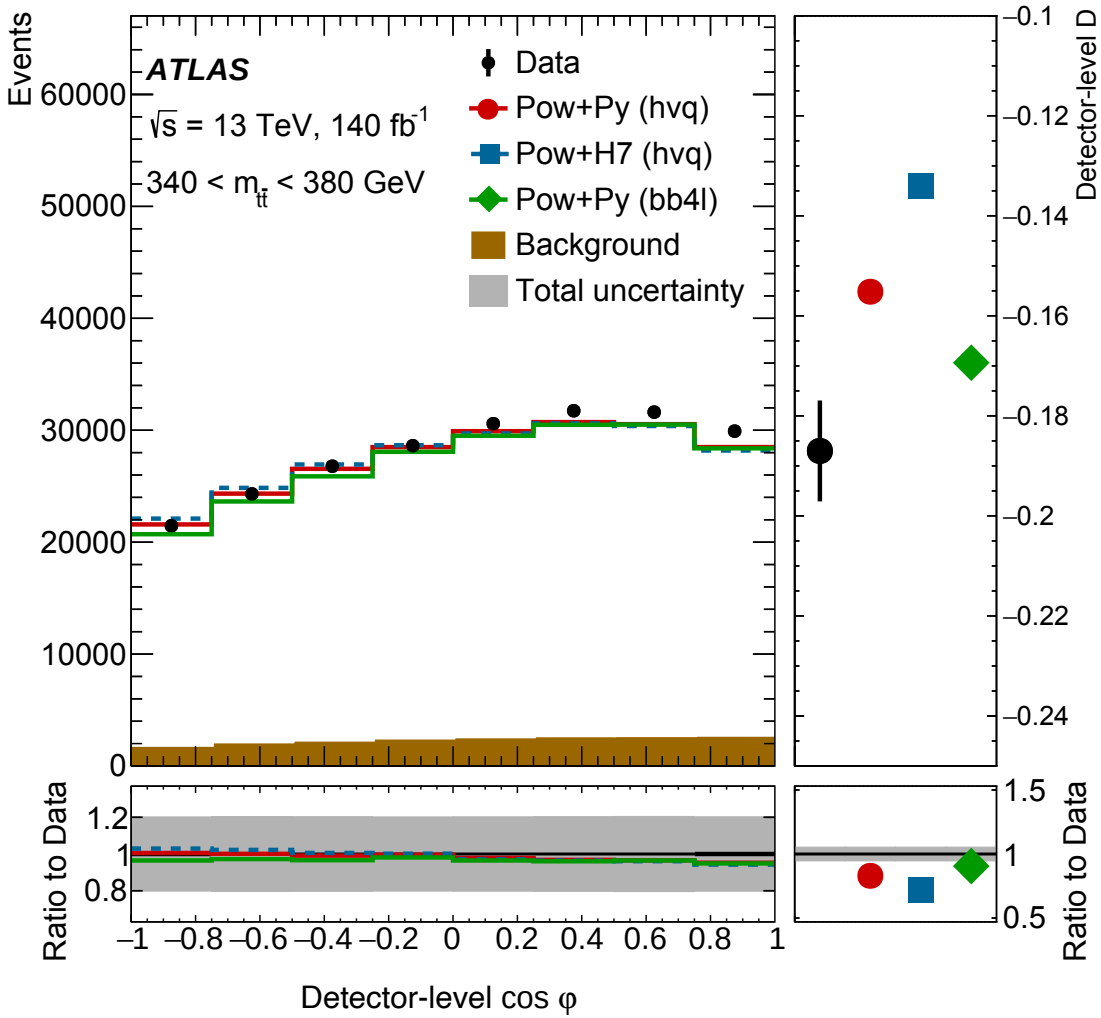
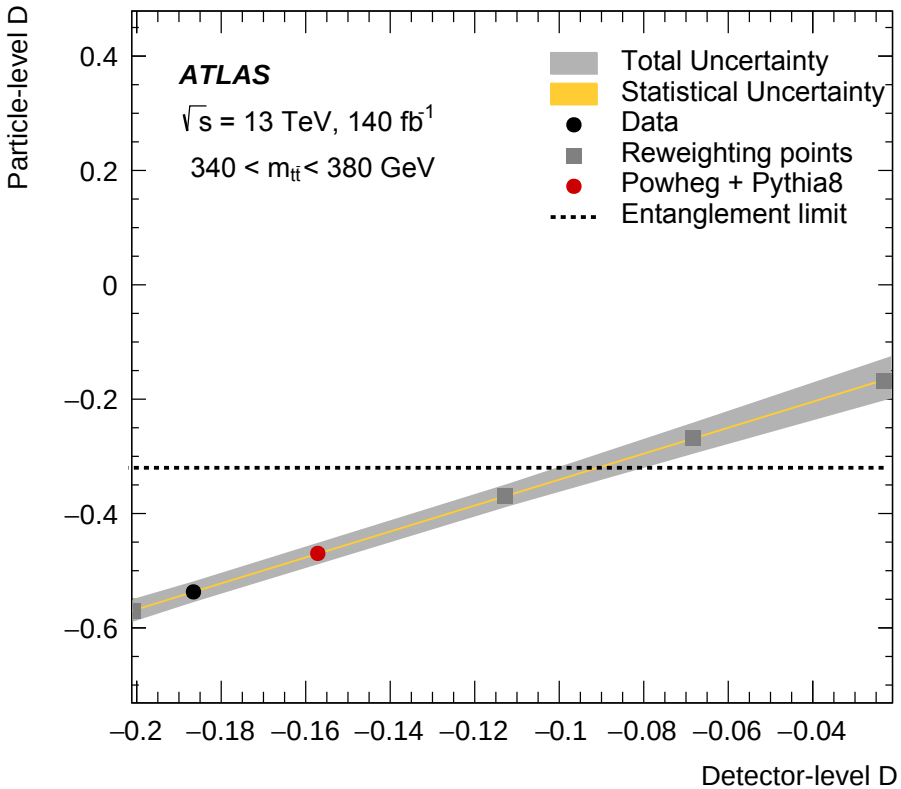


Figure: Observed lepton-angle distribution and detector-level entanglement marker.

ATLAS $t\bar{t}$ entanglement observation: calibration and validation

Nature 633 (2024) 542–547, 140 fb^{-1} at $\sqrt{s} = 13$ TeV



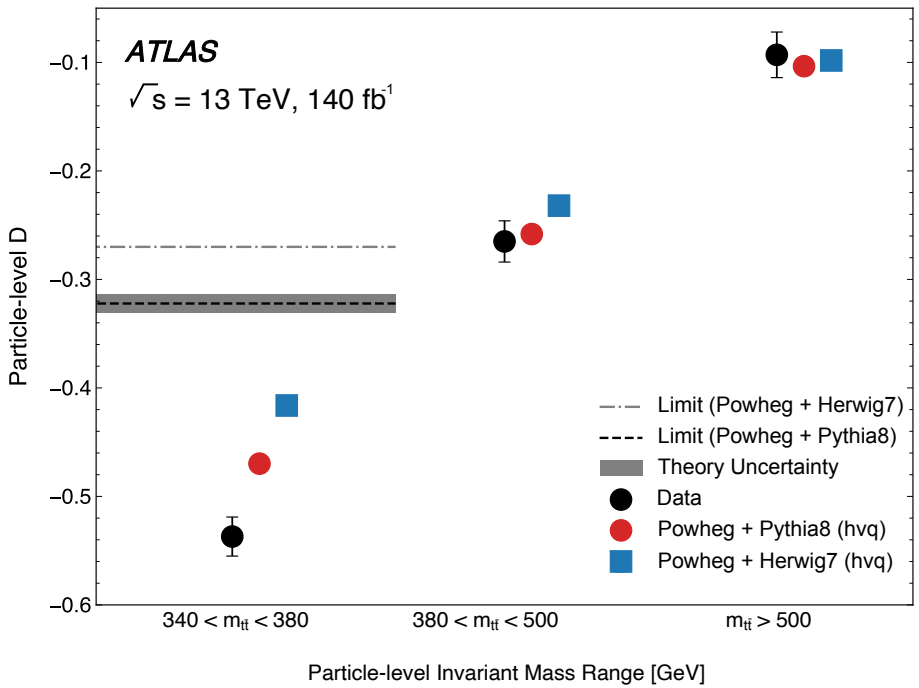


Figure: Calibration from detector-level to particle-level D (left); signal- and validation-region results against the entanglement limit (right).

ATLAS $t\bar{t}$ entanglement observation: uncertainty breakdown

Nature 633 (2024) 542–547, 140 fb^{-1} at $\sqrt{s} = 13$ TeV

Source	ΔD observed	ΔD expected
Signal modelling	0.017	0.015
Electrons	0.002	0.002
Muons	0.001	0.001
Jets	0.004	0.004
b-tagging	0.002	0.002
Pile-up	< 0.001	< 0.001
Missing transverse momentum	0.002	0.002
Backgrounds	0.005	0.005
Statistical	0.002	0.002
Systematic	0.019	0.017
Total	0.019	0.019

Table: Uncertainty breakdown for the entanglement marker D. The measured value is $D = -0.537 \pm 0.002$ (stat.) ± 0.019 (syst.), with the SM prediction of -0.470 ± 0.002 (stat.) ± 0.017 (syst.).

CMS $t\bar{t}$ entanglement observation: improved event selection

Rep. Prog. Phys. 87 (2024) 117801, 36.3 fb^{-1} at $\sqrt{s} = 13$ TeV

Differential dependence on Θ (top-quark production angle relative to the beam axis in the $t\bar{t}$ rest frame) and $\beta_z(t\bar{t})$ (longitudinal velocity of the $t\bar{t}$ system in the lab frame):

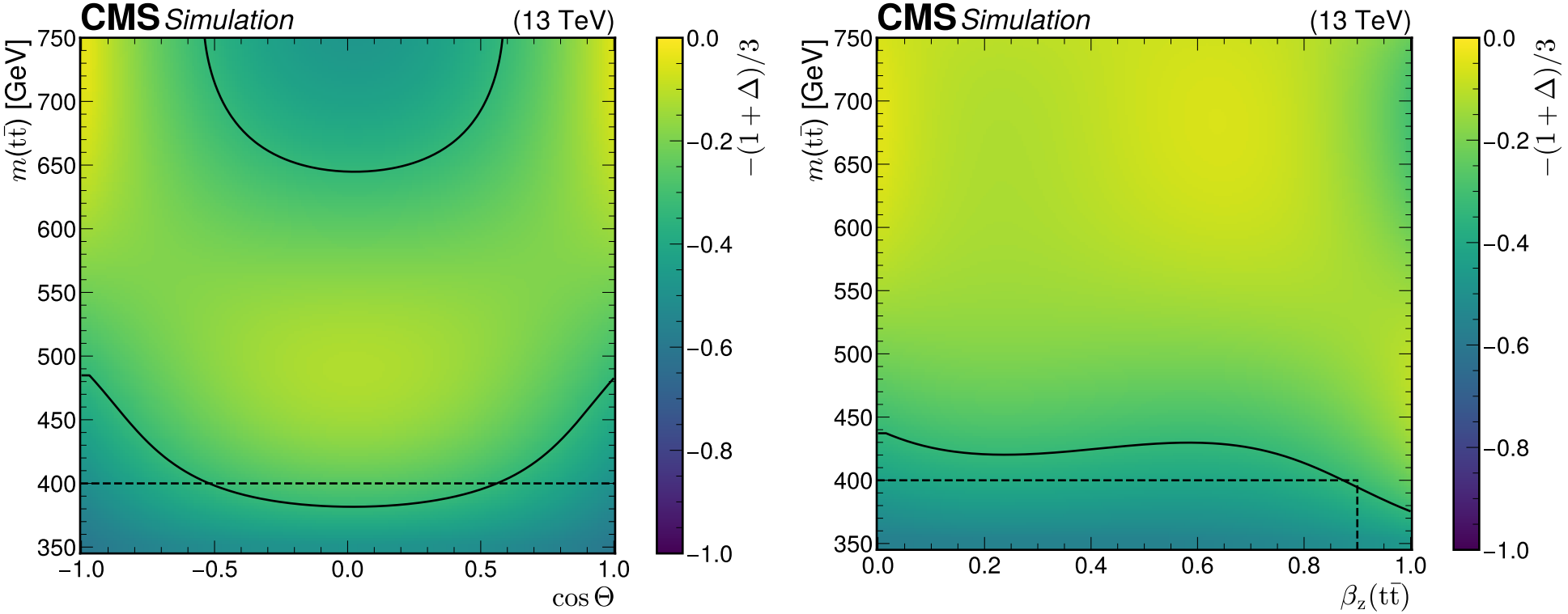


Figure: Predicted entanglement versus $m_{t\bar{t}}$ and $\cos\Theta$ (left), and $m_{t\bar{t}}$ and $\beta_z(t\bar{t})$ (right). Dashed lines indicate the selected region: $345 < m_{t\bar{t}} < 400$ GeV and $\beta_z(t\bar{t}) < 0.9$. The near-threshold selection maximizes entanglement sensitivity and suppresses $q\bar{q}$ production.

CMS $t\bar{t}$ entanglement observation: results and toponium-like effects

Rep. Prog. Phys. 87 (2024) 117801, 36.3 fb^{-1} at $\sqrt{s} = 13$ TeV

With η_t: $D = -0.480^{+0.026}_{-0.029}$, observed significance 5.1σ (with better data/MC agreement).
Without η_t: $D = -0.491^{+0.026}_{-0.025}$, observed significance 6.3σ.

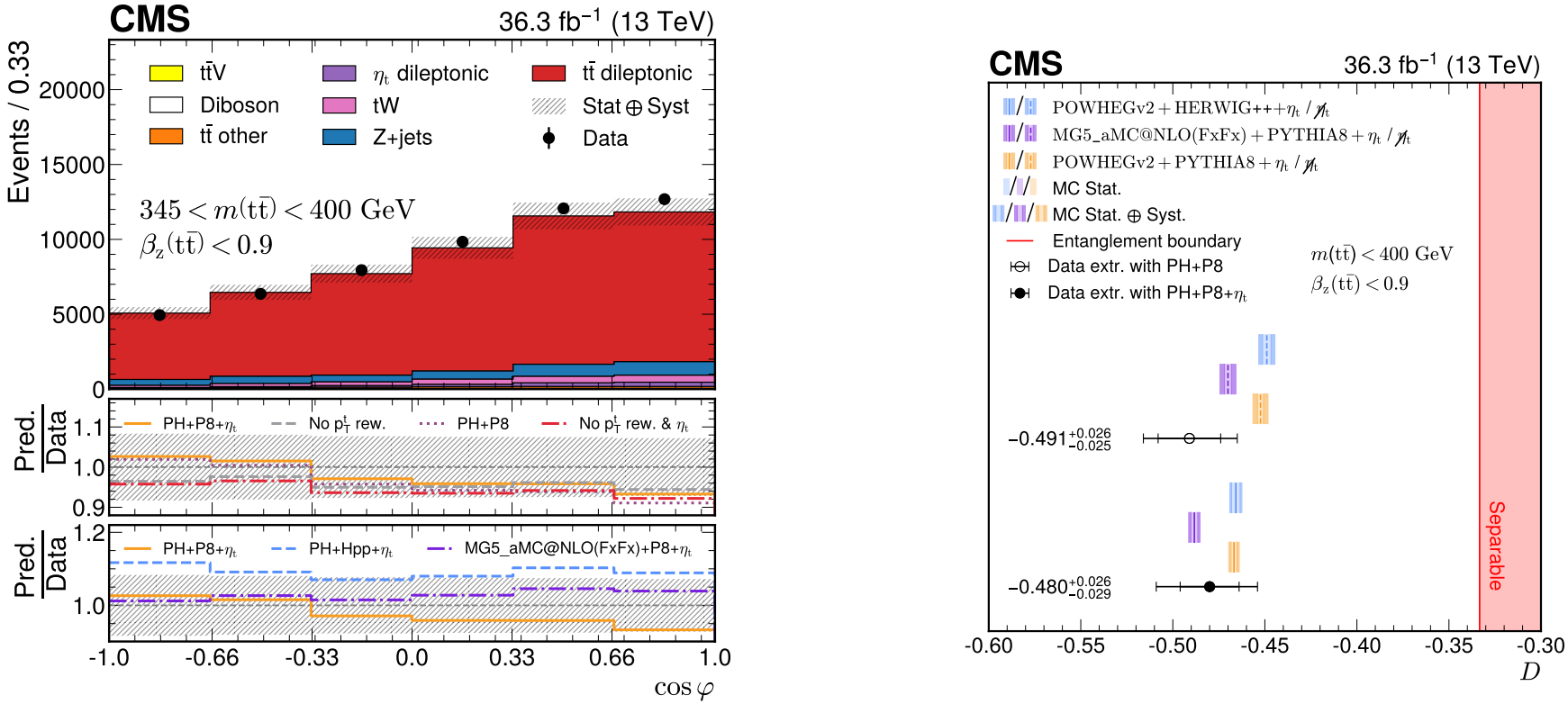


Figure: Reconstructed $\cos\varphi$ distribution (left). Measured D and predictions with (solid) and without (dashed) η_t; shaded band indicates the entanglement boundary (right).

CMS $t\bar{t}(b\bar{b}\ell\nu q\bar{q}')$ spin correlations: differential D

Phys. Rev. D 110, 112016 (2024), 138 fb^{-1} at $\sqrt{s} = 13$ TeV

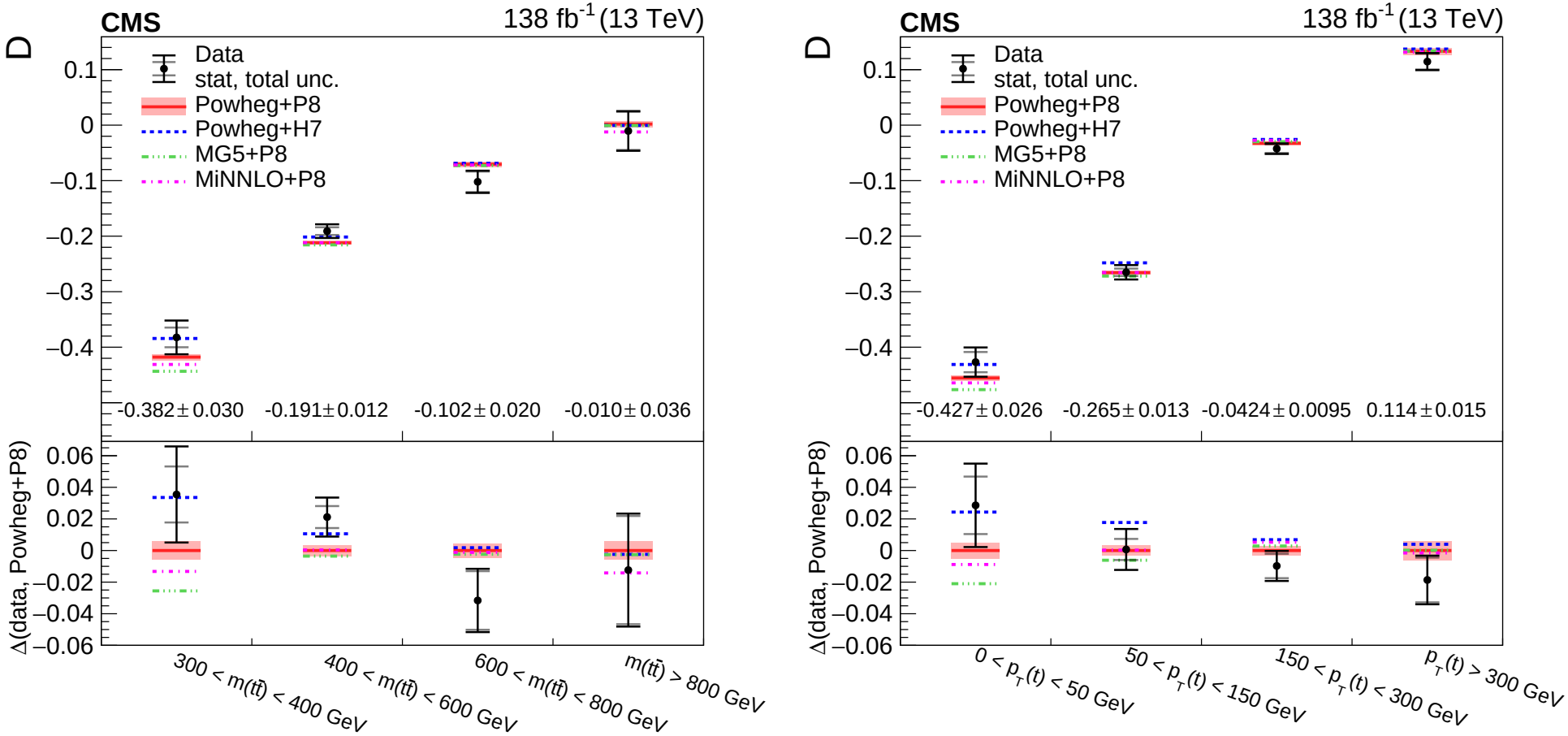


Figure: Differential D versus $m_{t\bar{t}}$ (left) and top-quark p_{T} (right), compared with SM predictions.

CMS $t\bar{t}(b\bar{b}\ell\nu q\bar{q}')$ spin correlations: differential $\tilde{D}$

Phys. Rev. D 110, 112016 (2024), 138 fb^{-1} at $\sqrt{s} = 13$ TeV

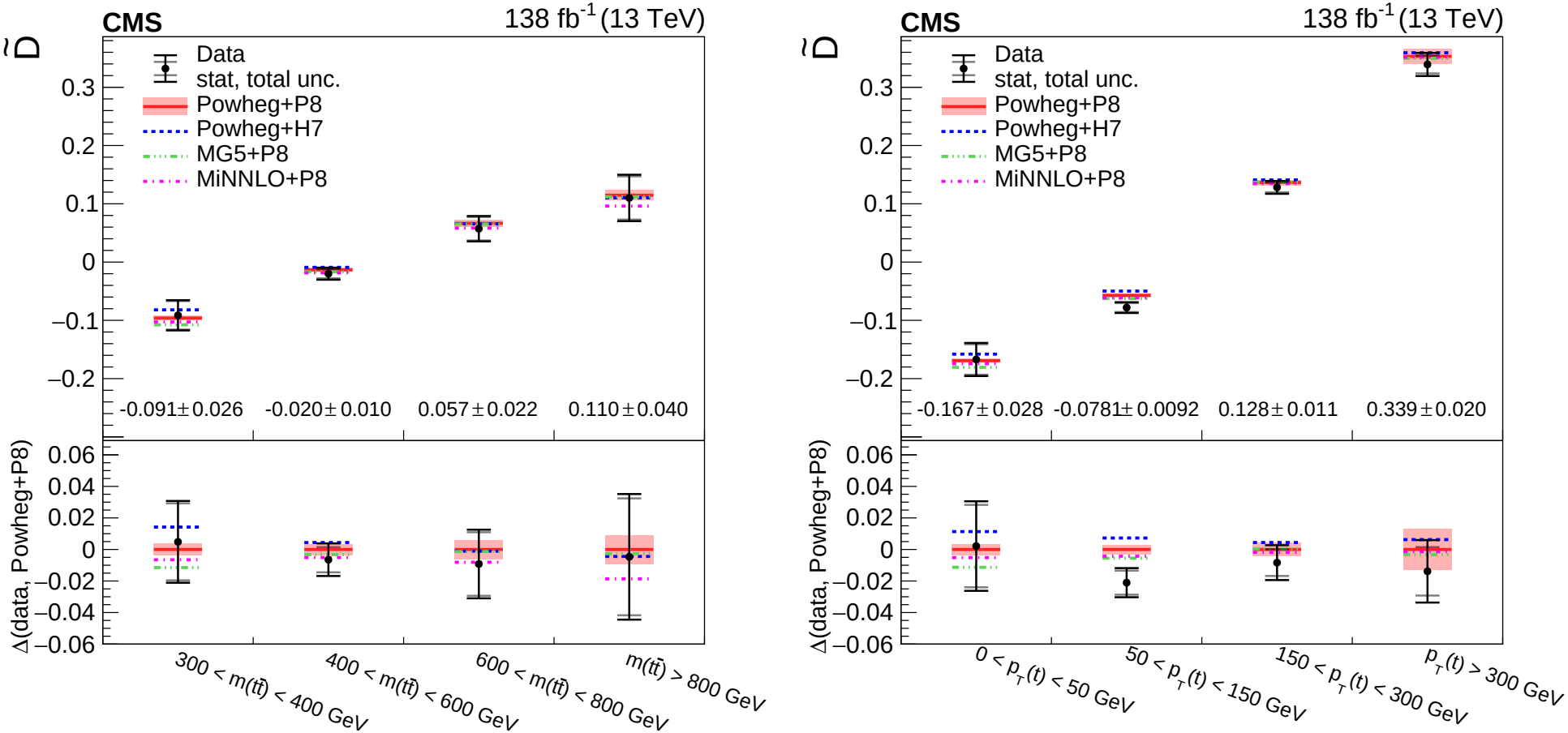


Figure: Differential $\tilde{D}$ versus $m_{t\bar{t}}$ (left) and top-quark p_{T} (right). Compared with $D = (C_{kk} + C_{rr} + C_{nn})/3$, sensitive to spin-singlet entanglement near threshold, $\tilde{D} = (C_{nn} - C_{rr} - C_{kk})/3$ probes spin-triplet entanglement at high energies.

CMS $t\bar{t}(b\bar{b}\ell\nu q\bar{q}')$ spin correlations: entanglement sensitivity

Phys. Rev. D 110, 112016 (2024), 138 fb^{-1} at $\sqrt{s} = 13$ TeV

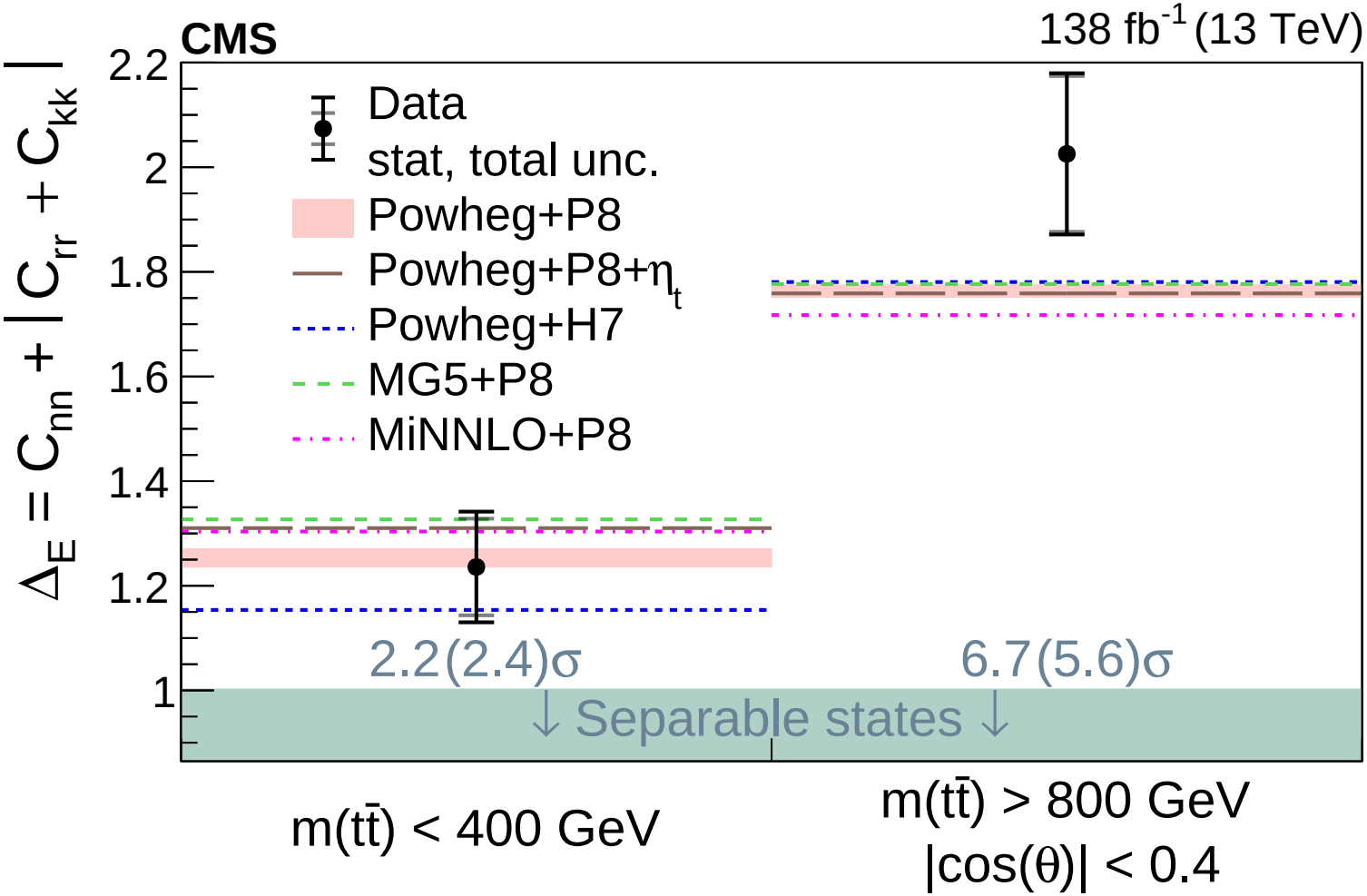
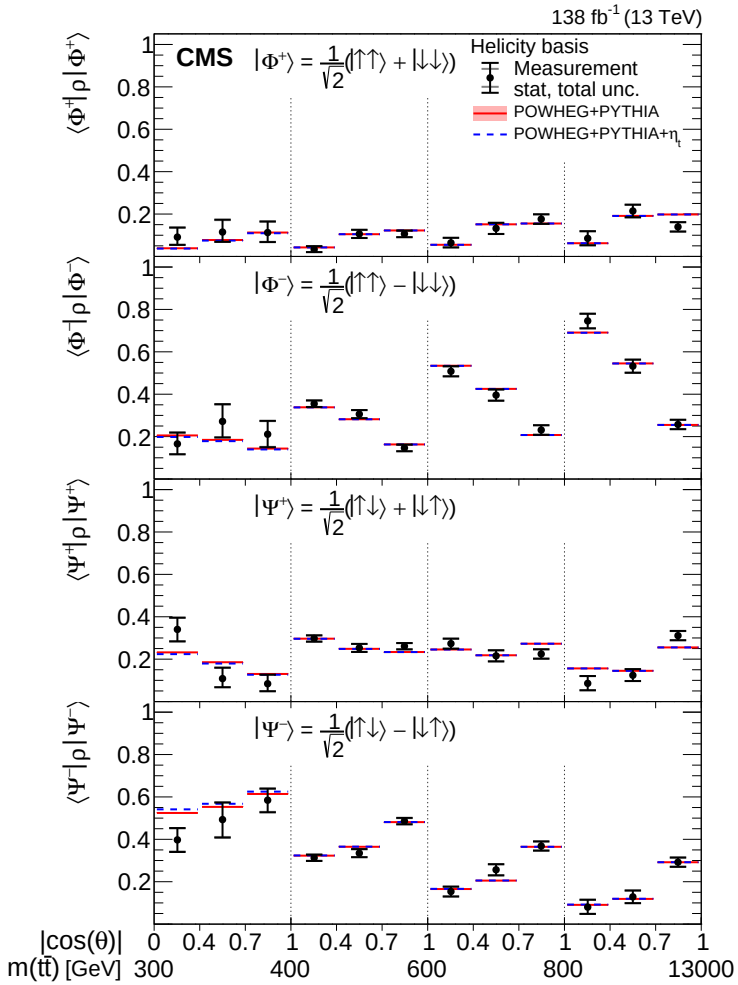


Figure: Entanglement-sensitive $\Delta_E = C_{nn} + |C_{rr} + C_{kk}|$ from the Peres–Horodecki criterion; $\Delta_E > 1$ indicates entanglement.

CMS $t\bar{t}$ spin-state measurements: decomposition

Phys. Rev. D 113, L051101 (2026), 138 fb^{-1} at $\sqrt{s} = 13$ TeV



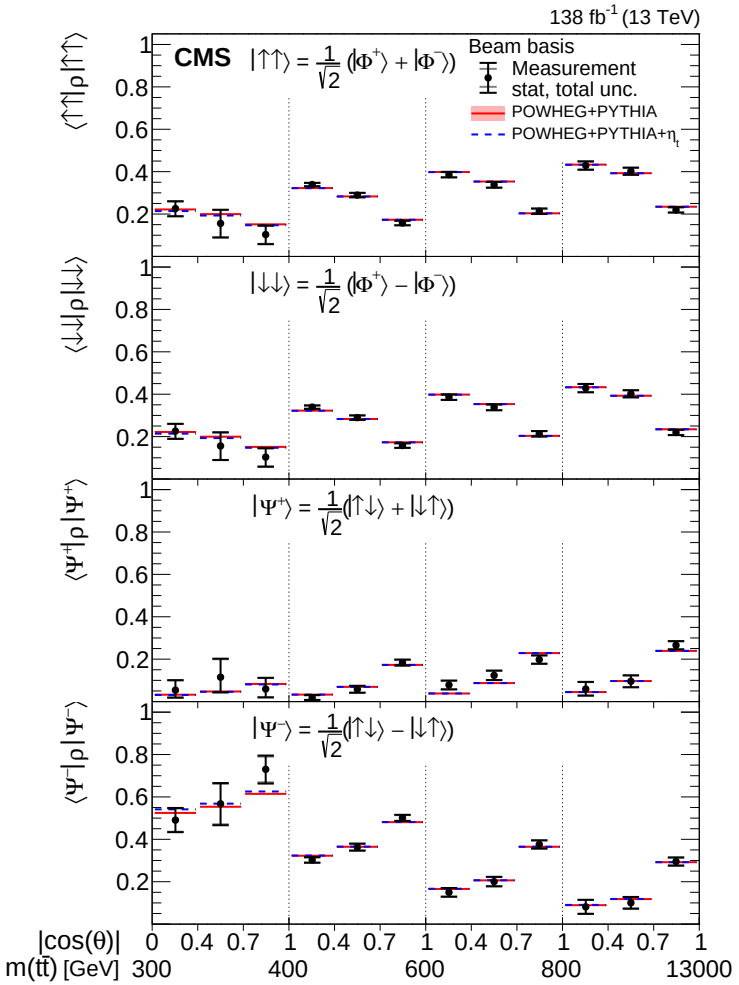


Figure: Density-matrix decomposition in the helicity (left) and beam (right) bases. The pseudoscalar state dominates near threshold (60–70%), while Φ^- dominates at high mass and central production ($\sim 70\%$). Consistent with the SM.

CMS $t\bar{t}$ spin-state measurements: purity and entropy

Phys. Rev. D 113, L051101 (2026), 138 fb^{-1} at $\sqrt{s} = 13$ TeV

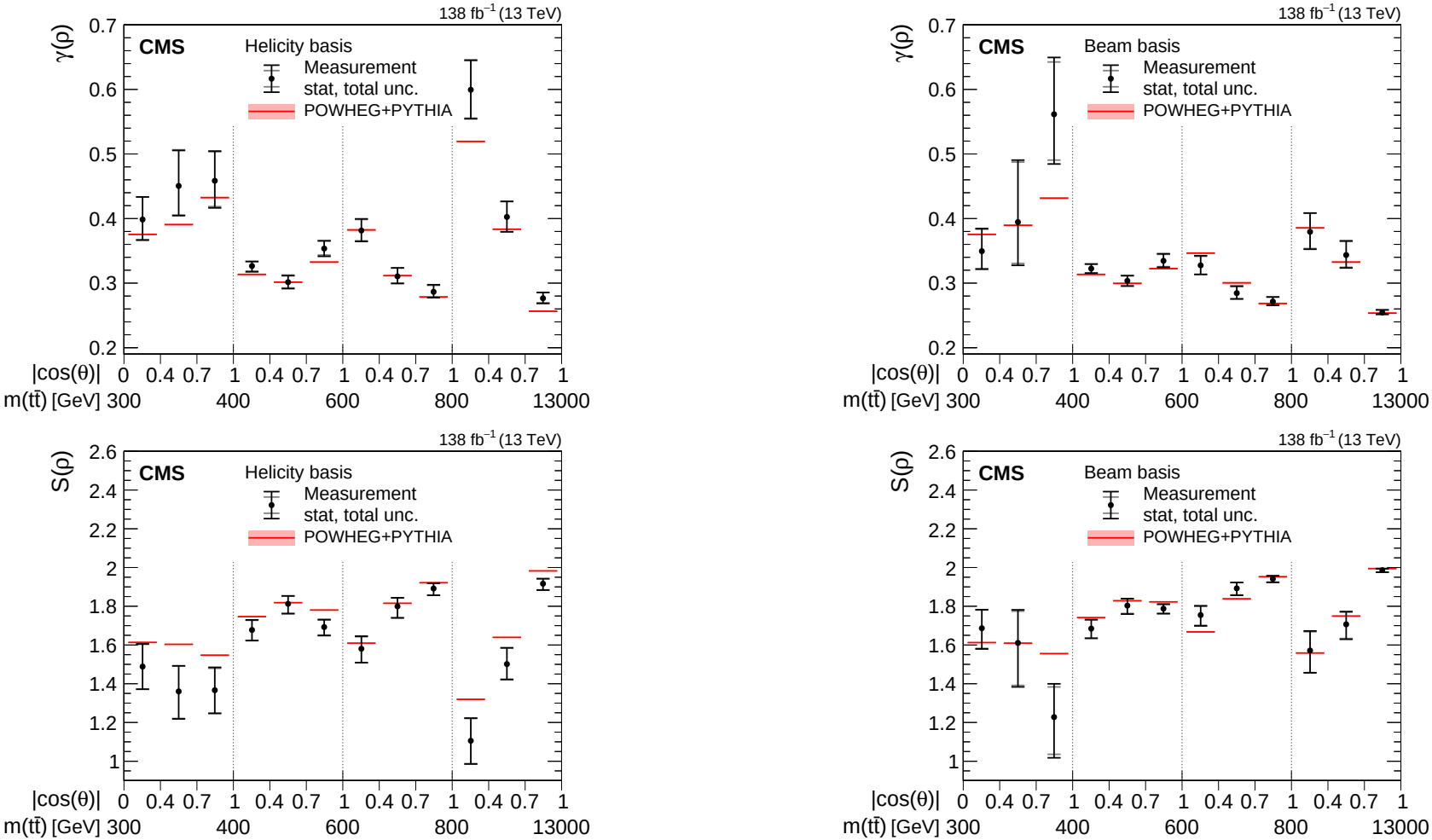


Figure: Purity $\gamma = \mathrm{Tr}(\rho^2)$ (top) and von Neumann entropy $S = -\mathrm{Tr}(\rho \log_2 \rho)$ (bottom), in helicity (left) and beam (right) bases. $(\gamma, S) = (1/4, 2)$ is maximally mixed and $(1, 0)$ is pure. These first experimental measurements agree with the SM.

CMS $t\bar{t}$ differential spin correlations: D and $D^{(n)}$ versus kinematics

CMS-PAS-TOP-23-006 (2026), 138 fb^{-1} at $\sqrt{s} = 13$ TeV

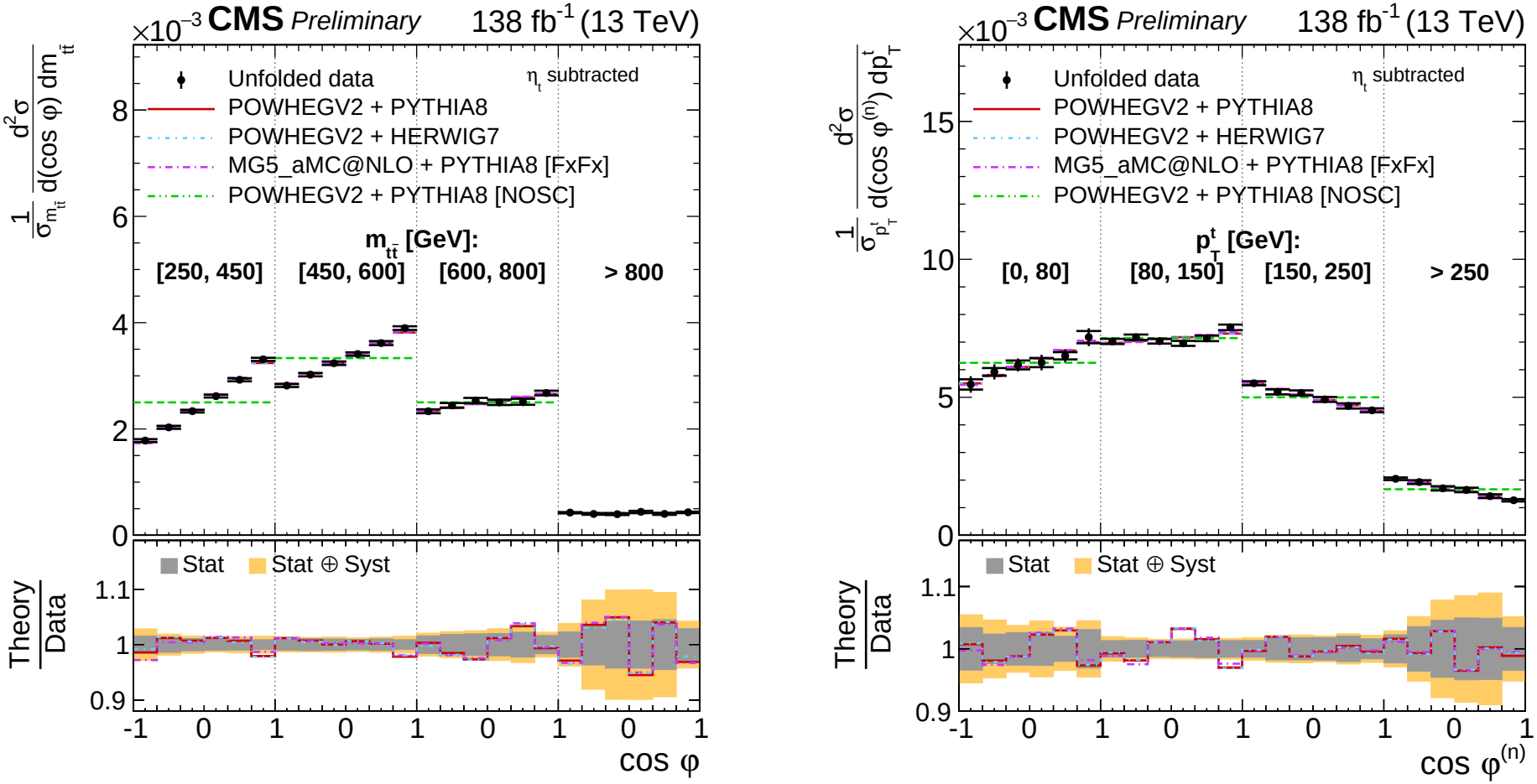
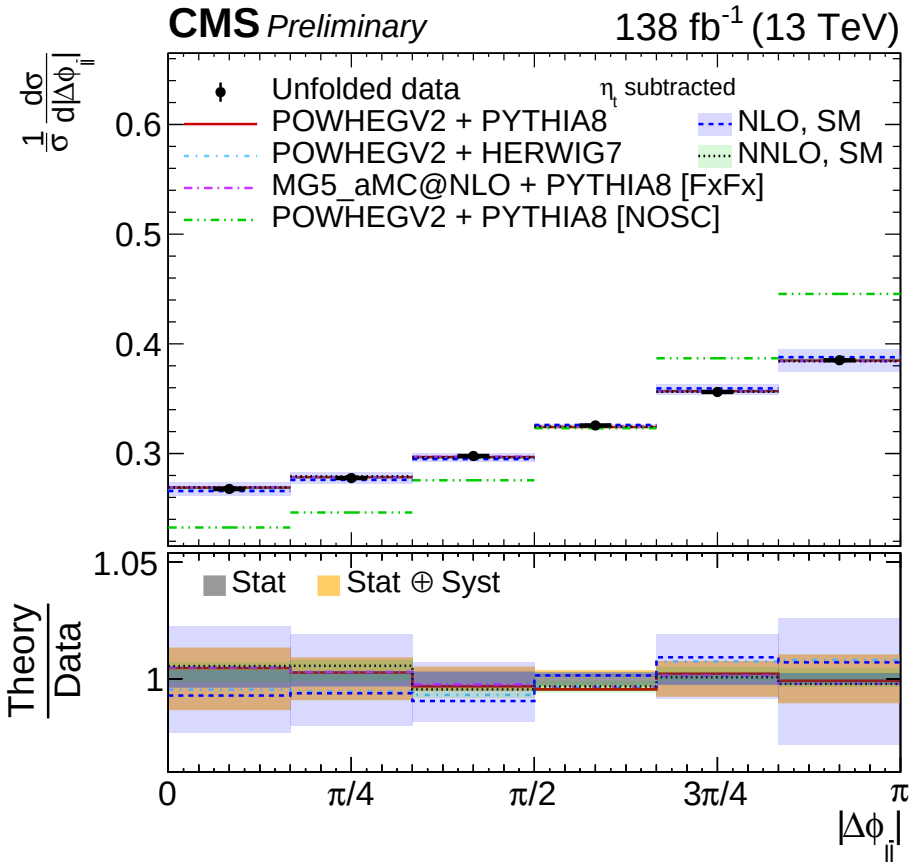


Figure: The measurements resolve D versus $m_{t\bar{t}}$ (left) and $D^{(n)}$ versus p_{T}^{t} (right); generator agreement varies with the kinematic binning.

CMS $t\bar{t}$ differential spin correlations: lab-frame $\Delta\phi_{\ell\ell}$ and $\Delta\eta_{\ell\ell}$

CMS-PAS-TOP-23-006 (2026), 138 fb^{-1} at $\sqrt{s} = 13$ TeV



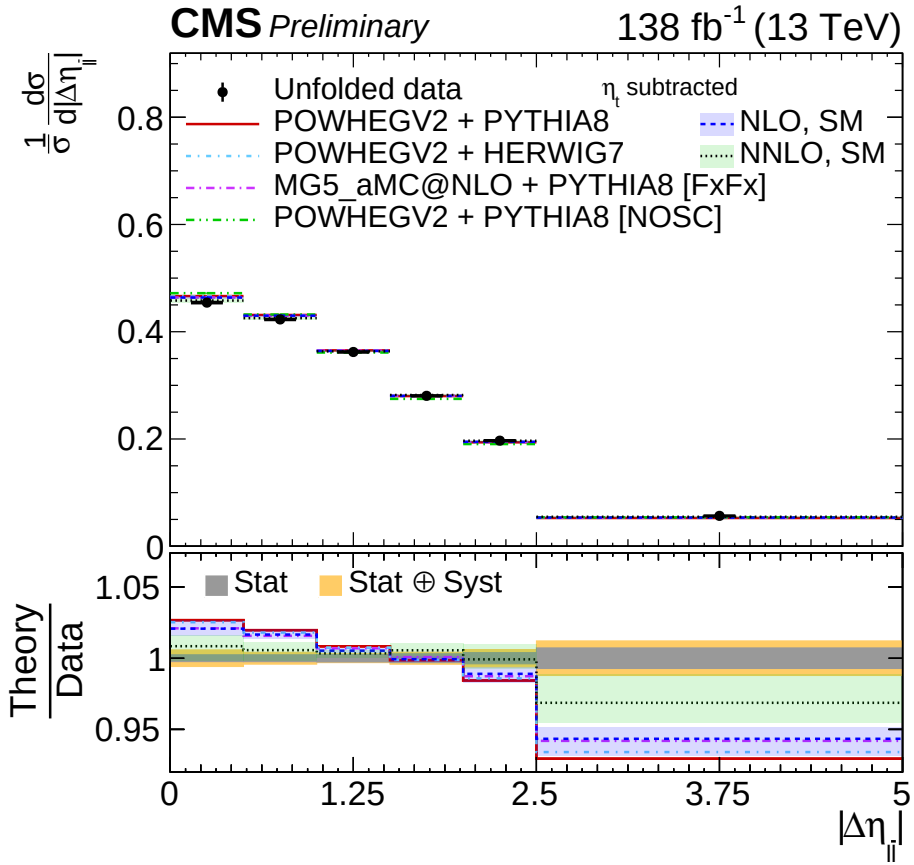


Figure: Left: $|\Delta\phi_{\ell\ell}|$; right: $|\Delta\eta_{\ell\ell}|$. The large-$|\Delta\eta|$ excess gives POWHEG+PYTHIA 8 $p = 2.4 \times 10^{-6}$. With theory uncertainties, fixed-order p improves from 0.0074 (NLO) to 0.22 (NNLO QCD).

$H \to ZZ^* \to 4\ell$: entanglement of Z-boson spins

HIG-25-011 (2025); Phys. Rev. Lett. 137, 111804 (2026)

- The clean, fully reconstructable $H \to ZZ^* \to 4\ell$ final state lets lepton momenta ideally probe the Z spins and reconstruct the spin density matrix ρ ($|\kappa_\ell| \approx 0.15$).
- Spin-density coefficients are deduced from angular moments:

$$C_{L_1,M_1,L_2,M_2} = \langle c_{L_1,M_1,L_2,M_2} \rangle, \qquad |M_i| \leq L_i.$$

- For a CP-even spin-0 Higgs at leading order, either nonzero coefficient signals entanglement:

$$C_{2,1,2,-1} \neq 0 \quad \text{or} \quad C_{2,2,2,-2} \neq 0 \quad \Longleftrightarrow \quad \rho \text{ entangled.}$$

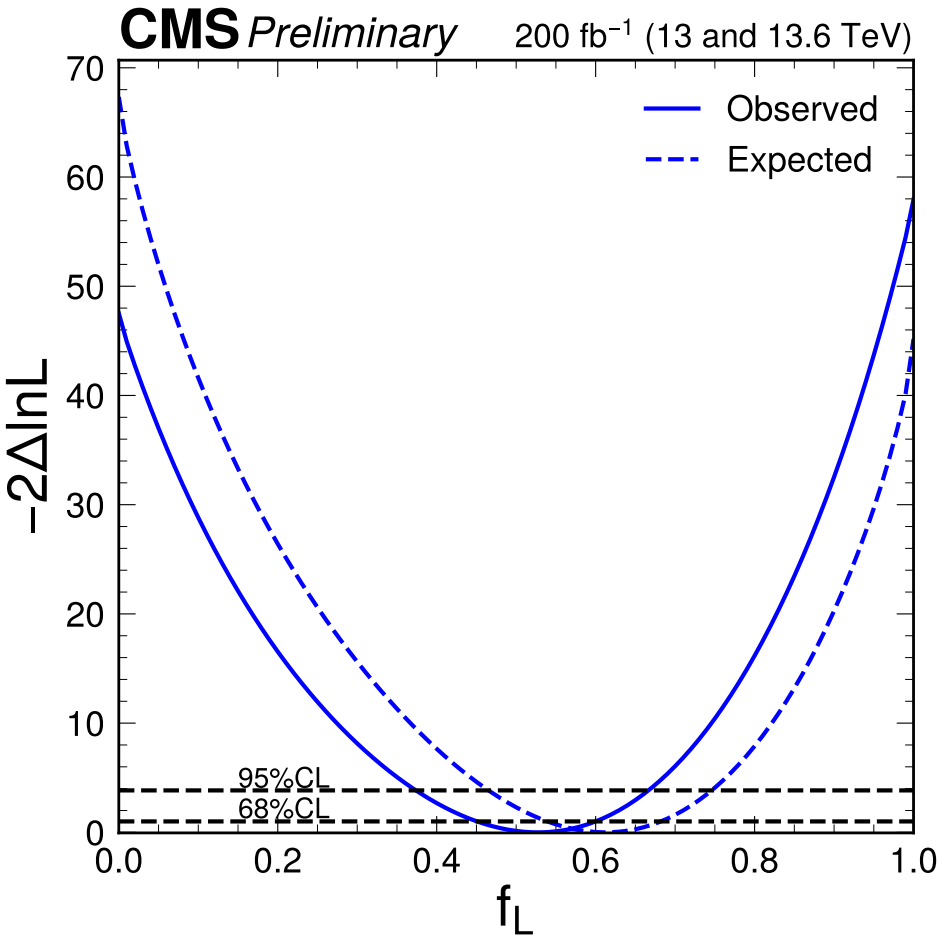
- A complementary CP-conserving polarization parameterization uses the longitudinal fraction f_L and longitudinal–transverse coherence $C_\parallel$:

$$f_\perp = 0, \qquad f_L + f_\parallel = 1, \qquad -1 \leq C_\parallel \leq 1.$$

$$C_{2,1,2,-1} = -3C_\parallel \sqrt{\frac{f_L(1-f_L)}{2}}, \qquad C_{2,2,2,-2} = \frac{3}{2}(1-f_L).$$

CMS $H \to ZZ^* \to 4\ell$: ZZ spin correlations

CMS-PAS-HIG-25-011 (2025), 138 fb^{-1} at 13 TeV and 62 fb^{-1} at 13.6 TeV



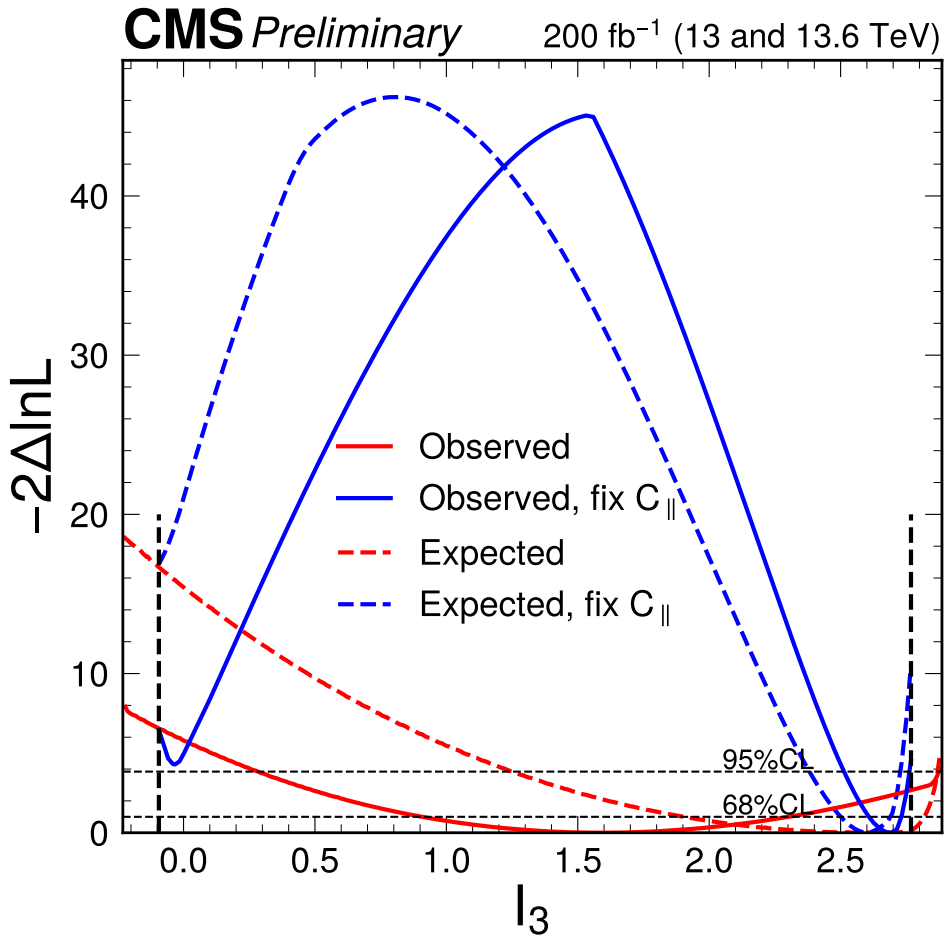
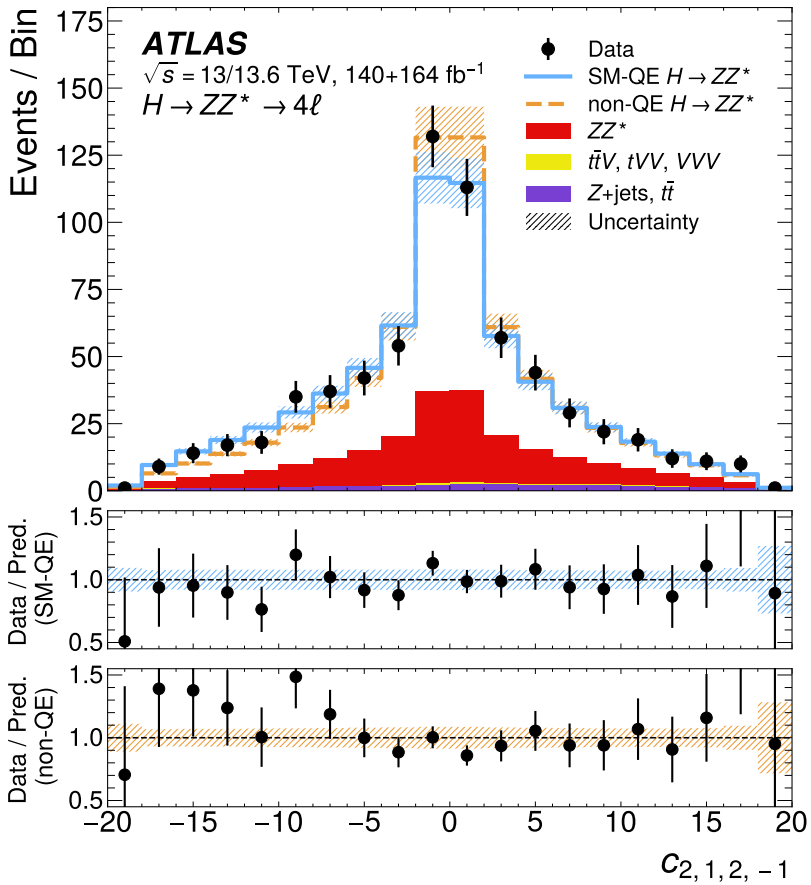


Figure: Assuming quantum mechanics and CP conservation, pure transverse and longitudinal states ($f_L = 0, 1$) are excluded at $> 6\sigma$ (left). $I_3 > 2$ reaches 95% CL only for large fixed $C_{\parallel}$; it is not established when $C_{\parallel}$ is unconstrained (right).

ATLAS $H \to ZZ^* \to 4\ell$: entanglement-sensitive spin-density coefficients

Phys. Rev. Lett. 137, 111804 (2026), 140 fb^{-1} at 13 TeV and 164 fb^{-1} at 13.6 TeV



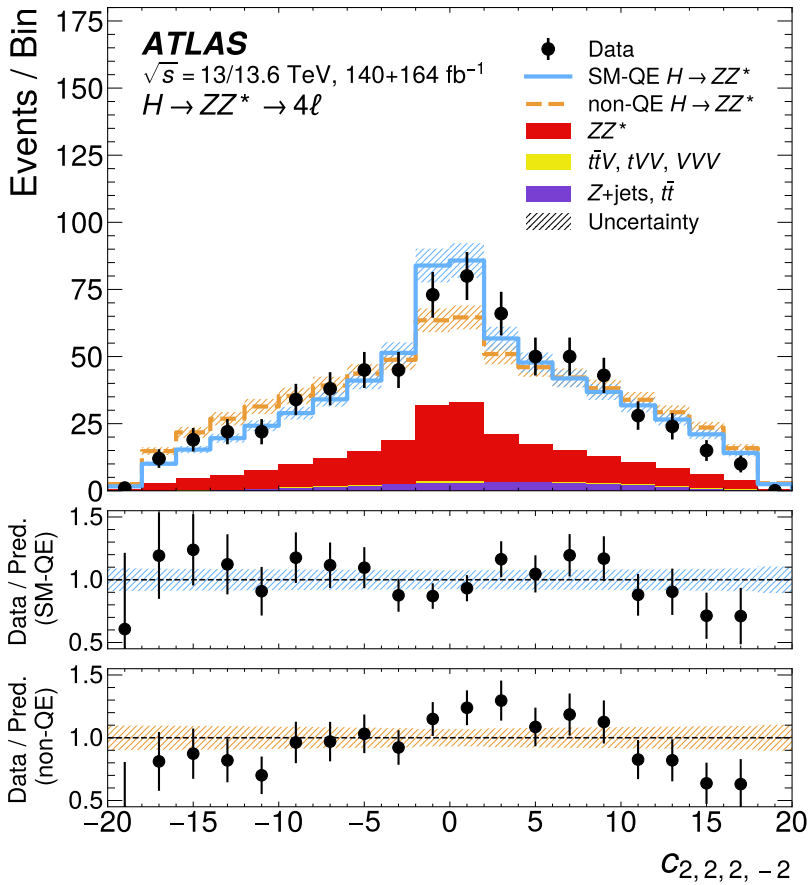


Figure: Observed $c_{2,1,2,-1}$ (left) and $c_{2,2,2,-2}$ (right) distributions. Combined fits: $C_{2,1,2,-1} = -0.71 \pm 0.45$ (SM: -0.97), $C_{2,2,2,-2} = 0.08 \pm 0.44$ (SM: 0.64); both are SM-consistent. The full-shape test rejects the separable $|00\rangle$ state at $4.7\,(4.9)\sigma$ observed (expected), assuming quantum mechanics, a CP-even scalar Higgs, and SM Z-decay angles.

Summary

- ATLAS and CMS observe $t\bar{t}$ entanglement near threshold. CMS also observes it at high mass: $6.7\,(5.6)\sigma$, exceeding the critical bound by $5.4\,(4.1)\sigma$ (obs./exp.).
- Differential top-pair measurements probe spin correlations across phase space; high-order correlations are proved to be important for accurate modeling.
- For $H \to ZZ^*$, ATLAS reports a 4.7σ rejection of the separable $|00\rangle$ state, while CMS establishes entanglement at $> 6\sigma$ assuming CP conservation.

Although loophole-free Bell tests remain challenging at current high-energy colliders, measurements of spin correlations provide a powerful probe of quantum entanglement, the coupling structure of the top quark and the Higgs boson, and the Standard Model from a new perspective.

Thanks for your attention!

Backup

Spin density matrix and measured coefficients

For a top and antitop spin-$1/2$ pair,

$$\rho = \frac{1}{4}\left[I \otimes I + \mathbf{B}^{+} \cdot \sigma \otimes I + I \otimes \mathbf{B}^{-} \cdot \sigma + \sum_{ij} C_{ij}\sigma_i \otimes \sigma_j\right].$$

- $\mathbf{B}^{\pm}$: polarization of top and antitop.
- C_{ij}: spin correlations along axes i, j.

CMS entanglement markers for near-threshold $t\bar{t}$ measurements

The four markers are defined from the diagonal spin-correlation coefficients as

$$D = \frac{-C_{kk} - C_{rr} - C_{nn}}{3}, \qquad D^{(k)} = \frac{C_{kk} - C_{rr} - C_{nn}}{3},$$

$$D^{(r)} = \frac{-C_{kk} + C_{rr} - C_{nn}}{3}, \qquad D^{(n)} = \frac{-C_{kk} - C_{rr} + C_{nn}}{3}.$$

- The definitions imply $D = D^{(k)} + D^{(r)} + D^{(n)}$.
- CMS measured $D = -23.1\%$, $D^{(k)} = -1.5\%$, $D^{(r)} = -19.0\%$, and $D^{(n)} = -2.3\%$.

CMS entanglement markers for high-mass $t\bar{t}$ measurements

CMS applies the Peres–Horodecki criterion to the measured spin-correlation matrix:

$$\Delta_E = C_{nn} + |C_{rr} + C_{kk}| > 1.$$

- Near threshold, C_{rr} and C_{kk} are positive, so $\Delta_E = \mathrm{Tr}(C) = -3D$.
- At high $m_{t\bar{t}}$, C_{rr} and C_{kk} become negative. CMS uses $\tilde{D} = (C_{nn} - C_{rr} - C_{kk})/3$, giving $\Delta_E = 3\tilde{D} > 1$.
- For the critical-entanglement bound, CMS uses the space-like decay fraction f:

  $$\Delta_{E,\mathrm{crit}} = f\Delta_{E,\mathrm{sep}} + (1-f)\Delta_{E,\mathrm{max}}, \qquad \Delta_{E,\mathrm{sep}} = 1, \quad \Delta_{E,\mathrm{max}} = 3.$$

  For $f = 90\%$, $\Delta_{E,\mathrm{crit}} = 1.2$.

CMS $t\bar{t}(b\bar{b}\ell\nu q\bar{q}')$ spin correlations: entanglement sensitivity

Phys. Rev. D 110, 112016 (2024), 138 fb^{-1} at $\sqrt{s} = 13$ TeV

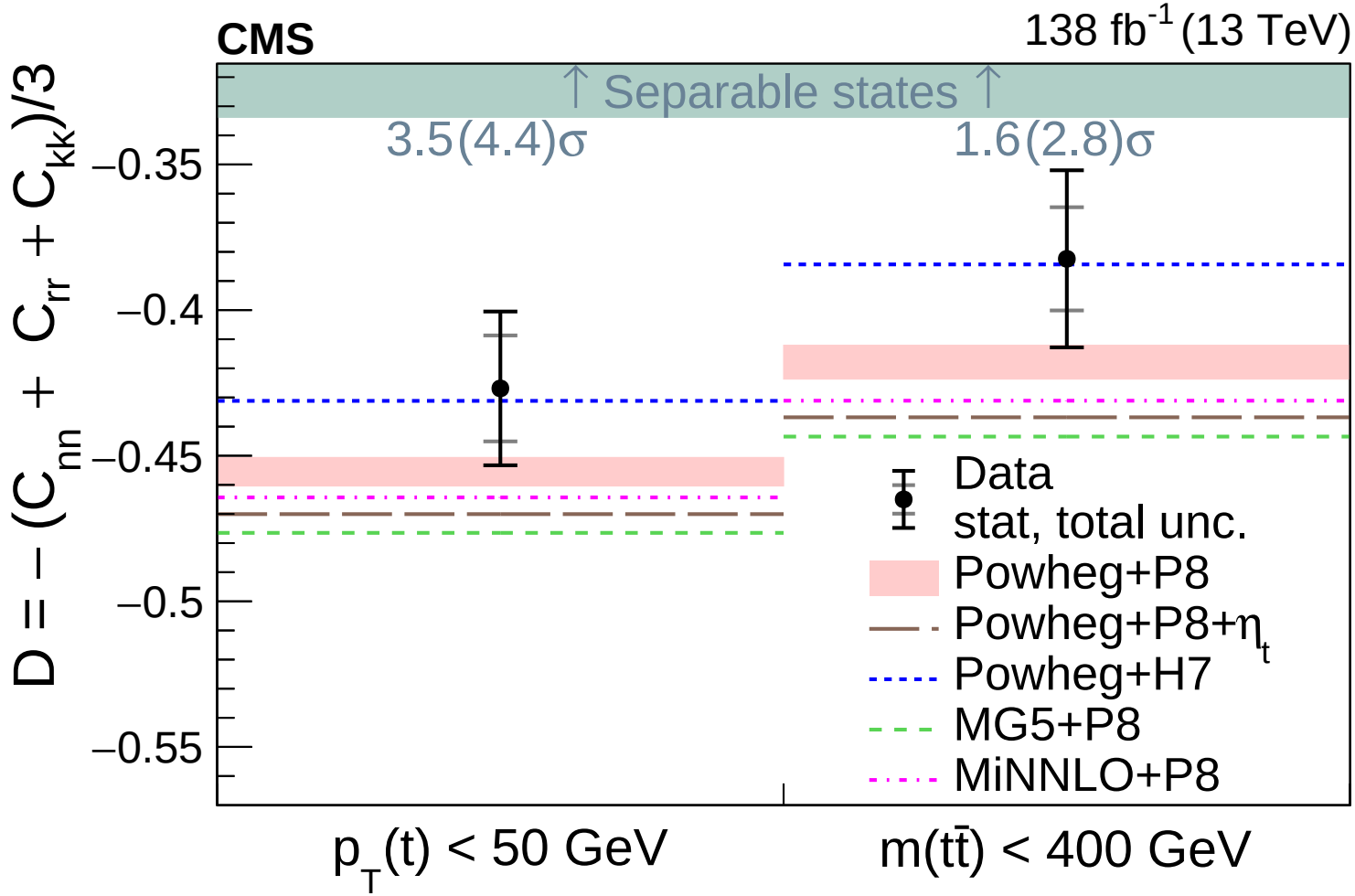


Figure: Entanglement-sensitive D near threshold.

CMS $t\bar{t}(b\bar{b}\ell\nu q\bar{q}')$ spin correlations: entanglement sensitivity

Phys. Rev. D 110, 112016 (2024), 138 fb^{-1} at $\sqrt{s} = 13$ TeV

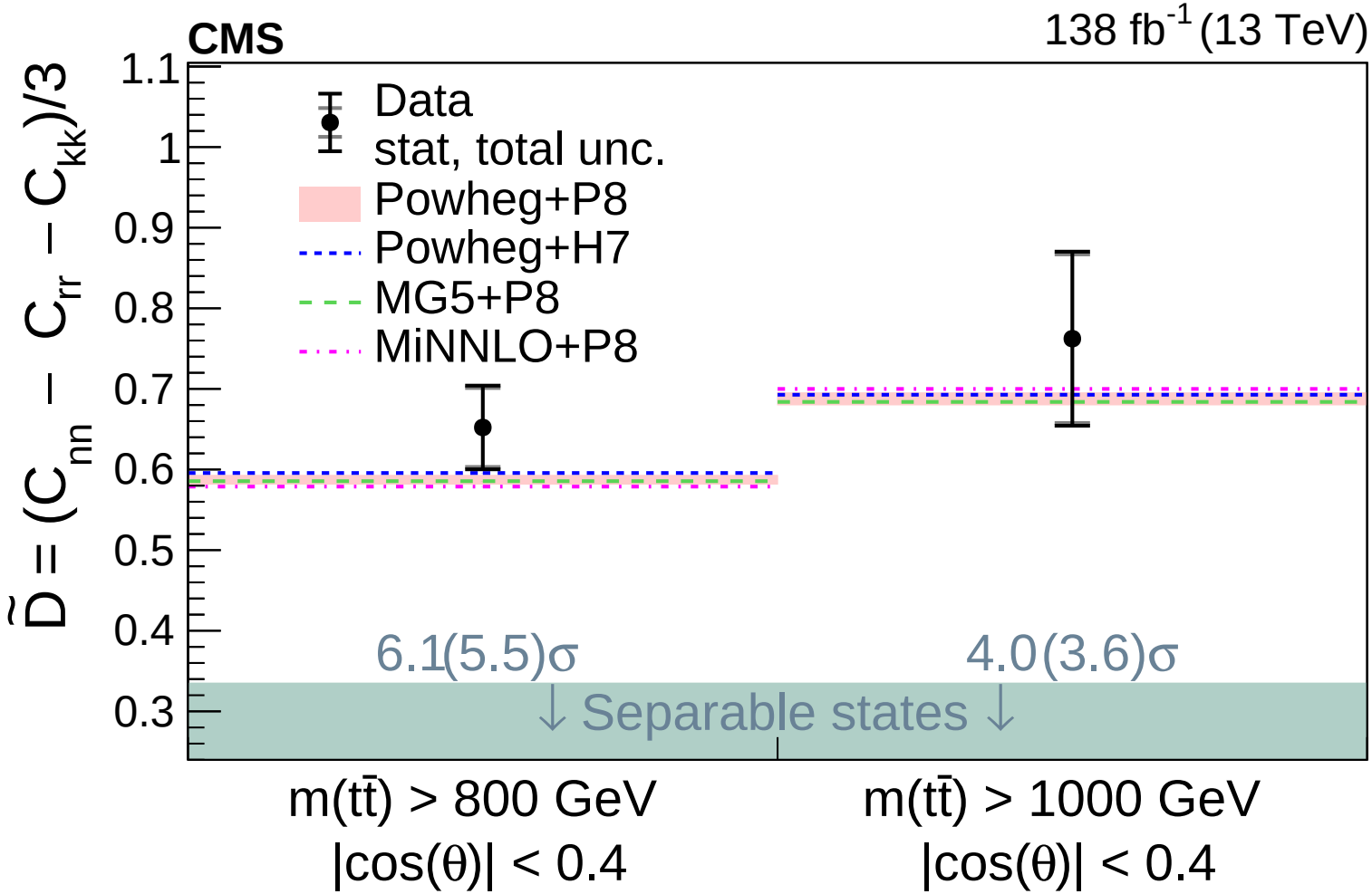


Figure: Entanglement-sensitive $\tilde{D}$ at high mass.

ATLAS+CMS $t\bar{t}$ spin correlations: combined $\Delta\phi_{\ell\ell}$ measurement

CMS-PAS-TOP-22-004 / ATLAS-CONF-2026-001, 36.1 + 35.9 fb^{-1} at $\sqrt{s} = 13$ TeV

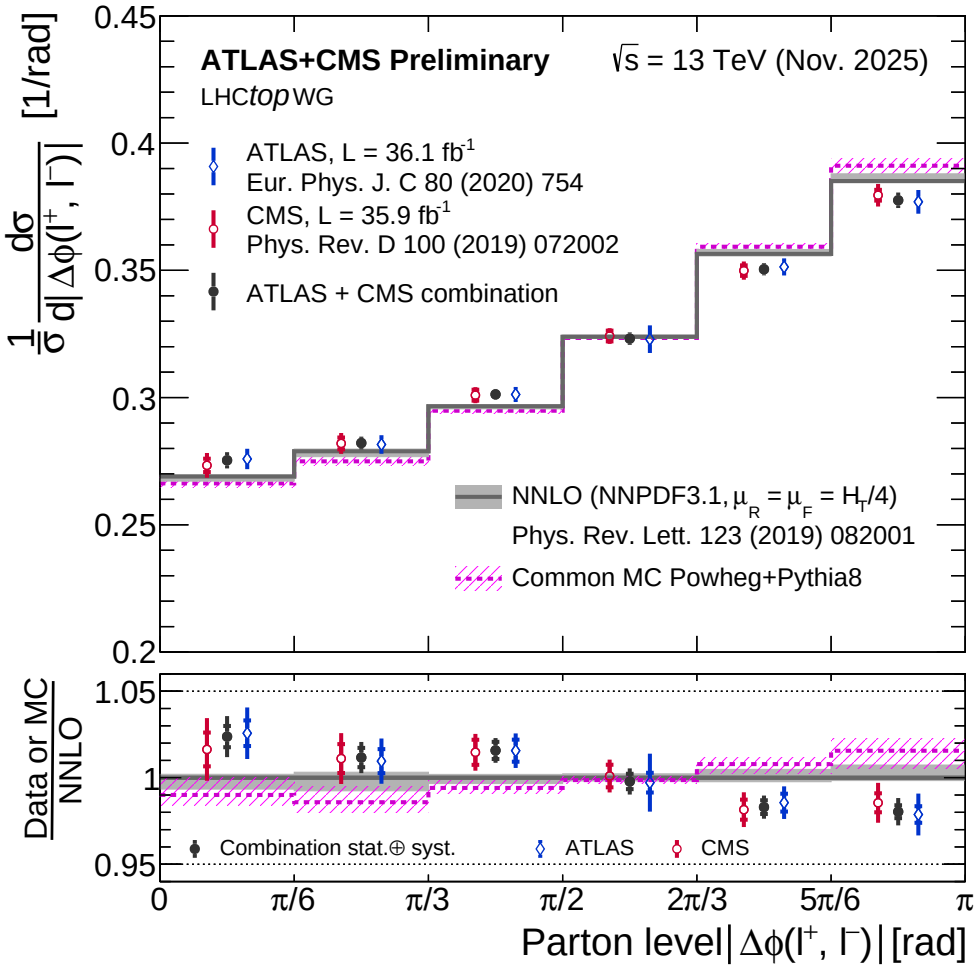


Figure: The combination reduces uncertainty in every bin; the data also show a shape difference from common POWHEG+PYTHIA 8.

ATLAS+CMS $t\bar{t}$ spin correlations: comparison with theory

CMS-PAS-TOP-22-004 / ATLAS-CONF-2026-001, 36.1 + 35.9 fb^{-1} at $\sqrt{s} = 13$ TeV

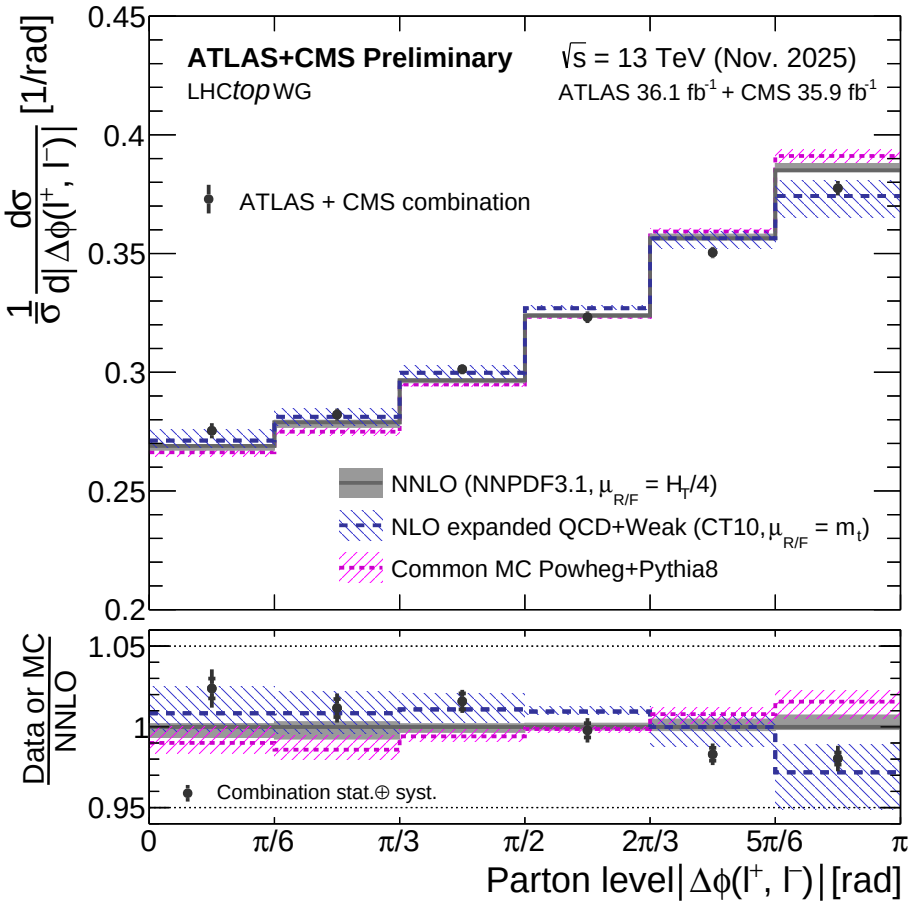


Figure: Combined measurement compared with theory predictions.

- Common NLO POWHEG+PYTHIA 8 poorly describes the data ($p = 2\%$).
- NNLO QCD: $p = 17\%$.
- NLO QCD+Weak: $p = 55\%$; larger scale uncertainty contributes to this higher value.
- The lower panel shows data and predictions relative to NNLO QCD.
- Fixed-order predictions agree better with the combined data.